TR-16-205

Nucleic Acids Research, 2016 ***1–15***
doi: 10.1093/nar/gkw825

A small stem-loop structure of the Ebola virus trailer is essential for replication and interacts with heat-shock protein A8

Joanna Sztuba-Solinska[1], Larissa Diaz[2], Mia R. Kumar[2], Gaëlle Kolb[2], Michael R. Wiley[3], Lucas Jozwick[3], Jens H. Kuhn[4], Gustavo Palacios[3], Sheli R. Radoshitzky[3], Stuart F. J. Le Grice[1,*] and Reed F. Johnson[2,*]

[1]RT Biochemistry Section, Basic Research Laboratory, National Cancer Institute-Frederick, National Institutes of Health, Fort Detrick, Frederick, MD 21702, USA, [2]Emerging Viral Pathogens Section, National Institute of Allergy and Infectious Disease, National Institutes of Health, Fort Detrick, Frederick, MD 21702, USA, [3]United States Army Medical Research Institute of Infectious Diseases, Fort Detrick, Frederick, MD 21702, USA and [4]Integrated Research Facility at Fort Detrick, National Institute of Allergy and Infectious Disease, National Institutes of Health, Fort Detrick, Frederick, MD 21702, USA

Received April 27, 2016; Revised September 7, 2016; Accepted September 8, 2016

ABSTRACT

Ebola virus (EBOV) is a single-stranded negative-sense RNA virus belonging to the *Filoviridae* family. The leader and trailer non-coding regions of the EBOV genome likely regulate its transcription, replication and progeny genome packaging. We investigated the *cis*-acting RNA signals involved in RNA–RNA and RNA–protein interactions that regulate replication of eGFP-encoding EBOV minigenomic RNA and identified heat shock cognate protein family A (HSC70) member 8 (HSPA8) as an EBOV trailer-interacting host protein. Mutational analysis of the trailer HSPA8 binding motif revealed that this interaction is essential for EBOV minigenome replication. Selective 2′-hydroxyl acylation analyzed by primer extension analysis of the secondary structure of the EBOV minigenomic RNA indicates formation of a small stem-loop composed of the HSPA8 motif, a 3′ stem-loop (nucleotides 1868–1890) that is similar to a previously identified structure in the replicative intermediate (RI) RNA and a panhandle domain involving a trailer-to-leader interaction. Results of minigenome assays and an EBOV reverse genetic system rescue support a role for both the panhandle domain and HSPA8 motif 1 in virus replication.

INTRODUCTION

Ebola virus (EBOV) can cause large and highly lethal human disease outbreaks. Because of the scarcity of effective treatments against EBOV, there is an urgent need to identify novel viral inhibitors that target specific viral processes. As of yet, relatively little is known about the molecular biology of EBOV replication, and in particular the interplay between host factors and the viral genome. The EBOV genome is a negative-sense, single-stranded RNA organized into a 3′ leader non-coding region (NCR), followed by seven discrete transcriptional units encoding NP (nucleocapsid protein), VP35 (polymerase cofactor and interferon-response modulator), VP40 (matrix protein), $GP_{1,2}$ (glycoprotein), VP30 (transcriptional enhancer), VP24 (secondary matrix protein, ion channel and interferon-response modulator), L (RNA-dependent RNA polymerase) and a 5′ trailer NCR (1,2). Each gene is separated by intergenic regions of varying lengths that modulate transcript levels (3).

The NCRs of RNA virus genomes have highly conserved primary and secondary structures (4–7). However, the functions of EBOV NCRs are not well characterized. Replicon systems consisting of the complete trailer and leader sequences and short segments of the L and NP protein genes that flank a reporter gene such as chloramphenicol acetyl transferase, green fluorescent protein, or luciferase have been developed (8–11). In these systems, transcription and replication from a replicon genome is supported by the EBOV proteins NP, L, VP35 and VP30, which are driven from co-transfected expression plasmids. Such systems allow examination of virus specific processes involving the RNA and these proteins. Addition of VP40 and GP expres-

*To whom correspondence should be addressed. Tel: +1 301 631 7200; Fax: +1 301 631 7389; Email: johnsonreed@mail.nih.gov
Correspondence may also be addressed to Stuart F. J. Le Grice. Tel: +1 301 846 5256; Fax: +1 301 846 6013; Email: legrices@mail.nih.gov

sion plasmids can drive production of infectious VLPs (10). Using the minigenome replicon systems and/or computer-assisted secondary structure predictions, some functions have been attributed to the NCRs. Computer modeling of the EBOV trailer and leader indicate that a panhandle structure may form between the NCRs starting with base paring of nucleotide (nt) 1 and 18 957. Almost identical hairpin structures for the leader of the EBOV genome and RI RNA are possible (12). Computer modeling of EBOV mini-RI RNA and mutational analysis suggested that the 3′-terminal 20 nts of the EBOV leader are not essential for infection (13). Chemical probing of the EBOV RI RNA revealed a stem-loop within the 5′ end that is involved in regulating transcription (14). Additional probing analyses of mini-RI RNA suggested that trailer and leader do not interact, but that the terminal 55 nts of the leader are important for replication (15). Recently, a direct interaction between VP30 and the 3′ leader has been described, suggesting that VP30 clamps the RNA template to prevent the polymerase complex (VP35/L) from dissociation and allows productive transcription initiation in the presence of secondary structures in the template (16,17). The optimal RNA substrate for VP30 binding is a single-stranded RNA that is linked to a stem-loop, as found in the region of the replication promoter element of the EBOV genomic leader (18). Other studies further emphasize the importance of non-terminal EBOV RNA secondary structures in transcription and replication. For instance, EBOV GP mRNA editing is dependent on such secondary structures (19–21). Interrupting secondary structure formation inhibits synthesis of the mRNA encoding $GP_{1,2}$, which mediates virion entry into host cells.

Host proteins bind to RNA secondary structures to modulate lifecycle processes for many positive-sense RNA viruses, such as hepatitis C virus (HCV) (22), hepatitis A virus (23), poliovirus type 1 (24), dengue viruses (25), bovine coronavirus (26) and murine hepatitis virus (27–29). However, few host protein–viral RNA interactions have been characterized for negative-sense, single-stranded RNA viruses. Previously, the La autoantigen (Sjögren syndrome antigen B) was shown to interact with the leader of rabies virus (30), vesicular stomatitis New Jersey virus (31,32) and rinderpest virus (32). La autoantigen is an RNA polymerase III transcription factor that shuttles between the nucleus and cytosol and may play a role in mRNA stability for translation. Interactions between the viral leader and La autoantigen are thought to play a role in replication. Replication is increased when the concentration of La autoantigen is increased (32) indicating a necessary functional role for host proteins to directly interact with the negative-sense viral genome. However, no specific viral RNA secondary structures that interact with La or other host proteins have been identified.

Host DNA topoisomerase 1 (TOP1) facilitates EBOV genome transcription and replication (33). In the case of retroviruses, such as human immunodeficiency virus-1 and Rous sarcoma virus, TOP1 interacts with their viral genome through a genomic RNA stem-loop, suggesting that TOP1-viral genome interaction directly regulates transcription and replication (34–36). Whether a similar interaction occurs with EBOV remains unclear, although, EBOV *NP* and *L* genes both contain a potential TOP1 target sequence (TCCTT) (33,37).

Considering the length (677 nt) and structural complexity of EBOV trailer, host and viral factors likely interact with trailer RNA motifs modulating the virus lifecycle. The goal of this study was to determine the secondary structure of the EBOV 3E-5E-enhanced GFP (3E-5E-GFP) minigenome RNA, identify host proteins that interact with the EBOV trailer, define their RNA binding motifs, and establish a functional role for the protein–RNA interactions. 3E-5E-GFP minigenome RNA secondary structure and host protein interactions were examined using selective 2′-hydroxyl acylation analyzed by primer extension (SHAPE) (38,39), antisense-interfered SHAPE (aiSHAPE) (40), electrophoretic mobility shift assays (EMSA), siRNA and mutational analysis, using both the 3E-5E-GFP minigenome system and EBOV reverse genetics.

MATERIALS AND METHODS

Cells and lysate preparation

The human kidney embryonic cell line, 293T (ATCC, Manassas, VA, CRL 3216) used in 3E-5E-GFP minigenome assays was maintained in Dulbecco's modified Eagle's medium (Lonza) supplemented with 10% calf serum (Sigma-Aldrich, St. Louis, MO, USA) with 1% v/v penicillin/streptomycin (LifeTechnologies, Grand Island, NY, USA) at 37°C in a 5% CO_2 atmosphere. HeLa cells (ATCC CCL-2) were similarly maintained and used for EBOV infection assays as described below. Grivet (*Chlorocebus aethiops*) Vero E6 cells (ATCC #CRL-1586) were maintained similarly and used for cell lysate preparation for EMSA as previously described (40). Lysates were collected by scraping 20 T-175 flasks of confluent cells into 20–30 ml of phosphate-buffered saline (PBS) followed by centrifugation at 1000 × *g* for 5 min. Pellets were resuspended in 2.5 ml of hypotonic buffer consisting of 10 mM HEPES (Sigma-Aldrich) 1.5 mM $MgCl_2$ (Sigma), 10 mM KCl (Sigma) and 0.2 mM PMSF (Sigma-Aldrich) and incubated on ice for 5 min. Non-ionic detergent (Igepal 620, Sigma-Aldrich) was added to a final concentration of 0.5% (v/v), and the suspension was vortexed twice for 30 s followed by incubation on ice for 10 min. The suspension was centrifuged at 3000 × *g* for 10 min to obtain a clarified lysate. Supernatant was removed and glycerol was added to a final concentration of 5% (v/v). Supernatants were aliquoted, frozen immediately on dry ice and stored at −80°C. A portion of the lysate was quantified using the Pierce BCA protein assay kit (Thermo Fisher Scientific, Waltham, MA, USA).

Polymerase chain reaction, *in vitro* transcription, site-directed mutagenesis and primers

Primers listed in Table 1 were used for EMSA template preparation, protein pull-down assays and site-directed mutagenesis for minigenome assays as indicated. Transcription templates for EMSAs were generated by polymerase chain reaction (PCR) amplification using the EBOV 3E-5E-GFP plasmid as a template. PCR products were resolved by 3–4.5% low melting temperature agarose gel electrophoresis

(Seakem GTG, Sigma-Aldrich) and purified using the QIAquick Gel Extraction Kit (Qiagen, Valencia, CA, USA). Products were dialyzed to remove excess salt and used as templates for transcription with the MEGAscript T7 kit (Thermo Fisher Scientific, Waltham, MA, USA) following the manufacturer's protocol. Radiolabeled probes were prepared by transcription in the presence of UTP-α^{32}P. Depending upon the length of the probe, they were purified by either phenol:chloroform extraction and ethanol precipitation or MEGAClear transcription clean-up kit (Thermo Fisher Scientific, Waltham, MA, USA), and subsequently quantified.

Electrophoretic mobility shift assays

Five microgram of protein lysate was incubated with 1.4 pmoles of radiolabeled probe in a final volume of 20 μl. Reactions were incubated at 22°C for 20 min in 1× reaction buffer consisting of 100 mM KCl, 10 mM Tris pH 7.6, 5 mM $MgCl_2$, 1 mM DTT, 500 ng Poly (I)-(C) (ThermoFIsher Waltham, MA, USA). Reactions with unlabeled specific wild-type (wt) competitor and non-specific tRNA competitor at 10, 25, 50 and 100× molar excess were carried out in parallel. The 20 μl reaction was loaded onto a 1× TBE, 6% non-denaturing polyacrylamide gel and electrophoresed for 2.5 h. Gels were transferred to Whatman 3CHR paper (Whatman Maidstone UK), dried at 80°C under vacuum for 2 h and exposed to a phosphorimager screen (GE Healthcare, Little Chalfont, UK). At least three independent assays were performed per probe. Typhoon 9410 software was used to analyze the gels and determine relative signal intensities of the shifted bands. Background subtracted signal intensity for each sample was determined as a ratio to wt in the absence of competitor. Relative average intensities were calculated and compared by paired *t*-tests using GraphPad Prism.

Protein pull-down and identification

The 1–116 probe (50 pmol) was biotinylated using the Pierce RNA 3′ End Biotinylation Kit (Thermo Fisher Scientific, Waltham, MA, USA) according to the manufacturer's protocol. This probe was purified by size-exclusion chromatography using ProbeQuant G-50 microcolumns (GE Healthcare Bio-Sciences) and incubated with streptavidin magnetic Dynabeads (Thermo Fisher Scientific, Waltham, MA, USA) in binding buffer for 1 h at 23°C with constant rocking. Lysate was prepared as described above and incubated with the prepared Dynabeads. Beads were harvested with a magnetic separator and washed in binding buffer three times. Protein was eluted by boiling in 2× lithium dodecyl sulfate buffer for 5 min. Samples were loaded on a 4–12% 3-(*N*-morpholino)propanesulfonic acid (MOPS) polyacrylamide gel and electrophoresed for 1 h at 200 V. The gel was silver-stained followed by mass-spectrometry of the whole lane for control and the 1–116 probe samples. Peptide fragments were generated, and protein identities were determined by amino acid sequence homology.

Immunoprecipitation-reverse transcriptase-PCR

Immunoprecipitation-Reverse Transcriptase-PCR (IP-RT-PCR) was performed as described previously (41). Briefly, Vero E6 lysate was incubated with 1–116 probe followed by immunoprecipitation with 0.5 μg of anti-HSPA8 (HSC70) antibody (SantaCruz Biotechnology, Dallas, TX, USA) and Protein G Dynabeads (Thermo Fisher Scientific, Waltham, MA, USA) and three rounds of washing with binding buffer. Bound material was eluted from the beads in 100 μl of elution buffer (50 mM Tris–HCl, pH 7.5, 10 mM EDTA, 1% sodium dodecyl sulphate (SDS)) at 70°C for 10 min. The eluate (20 μl) was loaded on SDS-MOPS 4–12% gels and probed for HSPA8. The remainder was digested by 96 μg of proteinase K for 30 min at 37°C, extracted by phenol:chloroform and precipitated with ethanol. The pellet was resuspended in 20 μl of deionized RNAse-DNase free water, and 500 pmol of the resuspension were reverse transcribed using Superscript III (Thermo Fisher Scientific, Waltham, MA, USA) followed by PCR with HiFi Taq (Thermo Fisher Scientific, Waltham, MA, USA) and the 1–116 primer set (Table 1). Negative control samples were processed in parallel by excluding the 1–116 RNA.

EBOV minigenome assays

The EBOV 3E-5E-GFP minigenome system was kindly provided by Dr Kawaoka, University of Wisconsin (10,42). The 1945 nt EBOV eGFP minigenome RNA comprises trailer (nt 1–677), a partial *NP* gene (nt 677–742), eGFP (nt 742–1455), a partial L gene (nt 1455–1891) and leader (nt 1891–1945) sequences. HEK 293T cells were seeded at 4.5 × 10^5 cells and incubated overnight at 37°C and 5% CO_2. Cells were transfected using the calcium phosphate method by combining an equal volume of a solution containing 0.25 M $CaCl_2$ and minigenome plasmids to 2× HBSS (0.28 M NaCl, 0.05 M HEPES, 0.0015 M $Na_2HPO_4 \cdot 7\ H_2O$) dropwise. The plasmids were in the following ratios per well: p3E-5E-GFP (1 μg), pCAGGSNP (500 ng), pCAGGSVP30 (300 ng), pCAGGSVP35 (500 ng), pCAGGSL (4 μg) and pT7 (1 μg). After 15 min incubation, the mixture was added to cells. At 48 h post-transfection, cells were harvested, washed and resuspended in 1% pluronic acid and 4% paraformaldehyde fixative for analysis by flow cytometry (Becton Dickenson, CA, USA). Measurements were gated relative to VP35-negative control samples. Statistical analysis was performed by one-way ANOVA using Graphpad Prism 6.0 (GraphPad Software).

Northern blot analysis

Total RNA from minigenome assay cells was extracted with TRIzol (Thermo Fisher). Five microgram of total RNA was DNase digested for 1 h at 37°C with RQ1 DNase (Promega). The RNA samples were electrophoresed for 1 h at 100 V in a 1× MOPS and 6% formaldehyde agarose gel and transferred to Hybond-N+ membrane (GE Healthcare). Probes specific for genomic and RI RNAs (Table 1) were labeled with ^{32}P ATP using T4 Polynucleotide Kinase (Promega). Membranes were prehybridized for 1 h in PerfectHyb Plus Buffer (Sigma Aldrich), and probe was added and hybridized overnight at 45°C for genomic and 55°C,

Table 1. Primers

Primers for EMSA assays EMSA probe name (nt)	Forward (5′-3′)	Reverse (5′-3′)
1-50	Taatacgactcactatagtggac	atggtcgcacacaaaaatttaaaaataaatc
1-116	taatacgactcactatagtggac	attgaccacgctcatcagaaggc
91-191	taatacgactcactatataggagc	actgtaaaatcagaaatacctt
180-319	taatacgactcactatataggattttac	tgtcgttttaaaaacggtga
288-411	taatacgactcactatataggattaag	cagatggaatagtgttttggtt
394-508	taatacgactcactatatagaaacac	gcaacataataaactctgca
504-627	taatacgactcactatatagttgcg	atttaaataacgaaaggagtccc
595-730	taatacgactcactatatagtataatatag	atagtatcctgatacttgcaa
A30URev	taatacgactcactatagtggac	gcacacaaaaatttaaaaaAaaatcta
Primers for single position nucleotide mutations for 3E-5E eGFP minigenome constructs		
Point mutation	**Forward (5′-3′)**	**Reverse (5′-3′)**
A26U	caaaaaagaagaaatagTtttatttttaaatttttg	caaaaatttaaaaataaActatttcttctttttttg
U27A	caaaaaagaagaaatagAttatttttaaatttttg	caaaaatttaaaaataaTtctatttcttctttttttg
U28A	caaaaaagaagaaatagatAtatttttaaatttttg	caaaaatttaaaaataTatctatttcttctttttttg
U29A	caaaaaagaagaaatagattAatttttaaatttttg	caaaaatttaaaaatTaatctatttcttctttttttg
A30U	caaaaaagaagaaatagatttTtttttaaatttttg	caaaaatttaaaaaAaaatctatttcttctttttttg
Primers for double mutations for 3E-5E eGFP minigenome constructs		
Mutations	**Forward (5′-3′)**	**Reverse (5′-3′)**
A26U/U27A	caaaaaagaagaaatagTAttatttttaaatttttg	
A26U/U27A		caaaaatttaaaaataTActatttcttctttttttg
A26U/U28A	caaaaaagaagaaatagTtAtatttttaaatttttg	
A26U/U28A		caaaaatttaaaaataTaActatttcttctttttttg
A26U/U29A	caaaaaagaagaaatagTttAatttttaaatttttg	
A26U/U29A		caaaaatttaaaaatTaaActatttcttctttttttg
A26U/A30U	caaaaaagaagaaatagTtttTtttttaaatttttg	
A26U/A30U		caaaaatttaaaaaAaaaActatttcttctttttttg
Northern blot probes:		
Genomic probe CGGTGATAGCCTTAATCTTTGTG		
Replicative Intermediate probe GGTTATTACACCTAATCTCTTATTTTACACAAAGATTAAGGCTA TCACCGTTTTTAAAACGACAAATTAAAGTAATGATAATTATAAAAAAC		
siRNA reagents		
Gene	**Catalog number**	**Vendor, catalog number**
HSPA8	On Target siRNA 4	Dharmacon/Thermo Scientific, LQ 017609060002
HSPA8	On Target siRNA 5	Dharmacon/Thermo Scientific, LQ-017609-07-0002
HSPA8	On Target siRNA 6	Dharmacon/Thermo Scientific, LQ-017609-08-0002
HSPA8	On Target siRNA 7	Dharmacon/Thermo Scientific, LQ-017609-09-0002
SHAPE primers		
Position (nt)	Name	Sequence
1925-1945	P1	cggacacacaaaaagaaagaag
1571-1592	P2	ccttggttttgaacttgaacac
1242-1263	P3	cttatggtgttcaatgcttttc
978-999	P4	cggcagacaaacaaaagaatgg
563-584	P5	cctctctccctgcgtgataatc
284-305	P6	ggtgatagccttaatctttgtg
LNA for aiSHAPE		
Position (nt)	Name	Sequence
1900-1912	3′_LNA1	+ctt+tt+gt +gtg+cga
1923-1938	3′_LNA2	+caa+aaa+ga+aa+gaa+gaa

3E-5E eGFP, 3E-5E plasmid containing enhanced green fluorescent protein; aiSHAPE, antisense-interfered SHAPE; EMSA, gel electrophoresis mobility shift assay; F, forward; LNA, Locked nucleic acid; R, reverse; SHAPE, selective 2′-hydroxyl acylation analyzed by primer extension.

respectively. Membranes were exposed to phosphor screen overnight and imaged on GE Typhoon FLA 9500 variable mode imager and quantified with ImageQuant software. Signal was normalized to VP35(-) sample for the genomic probe and normalized to WT sample for the RI probe.

siRNA screens

Various siRNAs targeting HSPA8 (Table 1) were used to transiently reverse-transfect HeLa cells (10 000 cells per well, 96-well format) in triplicate at a 30 nM final concentration, using HiPerfect (Qiagen) as previously described (43). Cells were washed the following day. Twenty-four hours later, cells were infected with EBOV-ZsGreen at MOIs of 20, 50 or 150 for 24 h. Cells were fixed with 10% formalin (Val Tech Diagnostics), and stained for high-content quantitative image-based analysis. The assay was repeated twice. In three wells on each plate, cells were transfected with a negative control siRNA (NT, siCONTROL Non-Targeting siRNA #2, Dharmacon D-001210-02).

EBOV reverse genetics

cDNA clones encoding EBOV/H.sapiens-tc/COD/1976/Yambuku-Mayinga (EBOV; GenBank #AF086833) wt and variants thereof (A30U, A26U/A30U or the 5′ terminal 50 nt deletion variant) were constructed by standard cloning techniques. For recovering recombinant viruses, HEK 293T cells in 6-well plates were transfected in duplicate with 1 μg of full-length EBOV cDNA clone-encoding plasmid and support plasmids (1 μg of pCAGGS-NP, 0.5 μg of pCAGGS-VP35, 0.3 μg of pCAGGS-VP30, 2 μg of pCAGGS-L and 1 μg of pCAGGS-T7) using Lipofectamine 2000 (Invitrogen Carlsbad, CA, USA) according to the manufacturer's instructions. As a negative control, pCAGGS-L was omitted from one of the samples. At day 5 post-transfection, supernatants were collected, cell debris was removed by centrifugation and an aliquot of the virus-containing media (termed passage 1) was used to infect a fresh monolayer of Vero E6 cells. One week later, when cytopathic effects were observed in the EBOV wt samples, supernatants (termed passage 2) were harvested, cleared by centrifugation and stored at −80°C. Vero E6 cells that did not exhibit cytopathic effects (those transfected with the EBOV mutants) were replenished with fresh growth media and incubated for an additional 3 days. Supernatants were harvested, cleared by centrifugation and stored at −80°C. All EBOV rescue experiments were conducted under Biosafety Laboratory 4 (BSL-4) conditions.

EBOV infections

Virus-containing supernatants (wt EBOV and mutants thereof) were used to infect Vero E6 or HeLa cells in 96-well plate (15 000 cells/well). Cells were inoculated with virus for 1 h, washed with PBS and replenished with fresh growth media. Cells were fixed 48 h later, blocked with 3% bovine serum albumin in PBS, stained with murine monoclonal antibodies against EBOV $GP_{1,2}$ (6D8, 1:1000 dilution) and with Alexa Fluor 488-conjugated antibodies (1:1000 dilution, Life Technologies). Infected cells were also stained with Hoechst 33342 and HCS CellMask DeepRed (Life Technologies) for nuclei and cytoplasm detection, respectively. Infection rates were determined by high-content quantitative image-based analysis on an Opera quadruple excitation high sensitivity confocal reader (model 3842 and 5025; Perkin-Elmer, Waltham, MA, USA) as described (44). All infections were conducted under BSL-4 conditions.

Sequencing

RNA was extracted using the Zymo DirectZol kit (Zymo Research) following the manufacturer's instructions, including the optional on-column DNase-treatment. RNA was prepared for sequencing and enriched for EBOV-specific reads using the Illumina TruSeq RNA Access kit with modifications to the manufacturer's recommended procedures as described previously (45). Libraries were sequenced on an Illumina MiSeq desktop sequencer using a version 2, 300 cycle kit (2 × 150) and analyzed using in-house scripts.

3E-5E-GFP minigenome RNA synthesis for SHAPE

DNA templates for *in vitro* transcription were generated by PCR amplification of plasmid encoding the EBOV 3E-5E-GFP minigenome and the corresponding replicon mutants, using primers listed in Table 1. All PCR experiments were performed using Platinum® Taq DNA polymerase High Fidelity (Thermo Fisher Scientific, Waltham, MA, USA). Transcripts were synthesized with the T7-MEGAscript system (Thermo Fisher Scientific, Waltham, MA, USA) following the manufacturer's protocol. RNAs were purified by denaturing 8 M urea/5% polyacrylamide gel electrophoresis, followed by elution and ethanol precipitation. Purified RNAs were dissolved in sterile water and stored at −20°C.

Selective 2′-hydroxyl acylation analyzed by primer extension

Six pmol of RNA was heated at 90°C for 3 min and slowly cooled to 4°C. The volume was adjusted to 150 μl in a final buffer of 50 mM Tris–HCl (pH 8.0), 100 mM NaCl, 5 mM $MgCl_2$. Samples were incubated at 37°C for 15 min. Folded RNA was divided into two equal portions (72 μl each) treated with 8 μl of 20 mM 1-methyl-7-nitroisatoic anhydride (1M7) (46) in anhydrous DMSO (+) or DMSO alone (−). Tubes were incubated at 37°C for 5 min, and RNA was precipitated at −20°C with 60 ng/μl of glycogen, 0.3 M sodium acetate (pH 5.2) and three volumes of cold ethanol. Precipitated RNA was collected by centrifugation and resuspended in 10 μl of water. SHAPE primers (3 pmol) labeled with Cy5 (for modified samples) or Cy5.5 (for unmodified samples) (Table 1) in 7 μl water were annealed to the RNA at 85°C for 1 min, 60°C for 5 min and 35°C for 5 min. RNA was reverse transcribed at 50°C for 50 min with 100 U of reverse transcriptase (Superscript III, Thermo Fisher Scientific, Waltham, MA, USA), 1× reverse transcription buffer, 5 mM DTT and 500 mM dNTPs (Promega). RNA was hydrolyzed with 200 mM NaOH for 5 min at 95°C, and reactions were neutralized with an equivalent volume of 2 M HCl. Sequencing ladders were prepared using the SequiTherm EXCEL DNA cycle sequencing kit (Epicentre, Madison, WI, USA) according to the

manufacturer's instructions. SHAPE primers were labeled with WellRED D2 and LI-COR IRDye-800 dyes. Modified and control samples were mixed with the sequencing ladders, precipitated as above, dried and resuspended in 30 μl of deionized formamide. Primer extension products were analyzed on a CEQ 8000 Genetic Analysis System (Beckman Coulter, Fullerton, CA, USA) as previously described (47). Electropherograms were processed using the open-source SHAPEfinder program ver. 1.0 following the software developer's protocol, including the required precalibration for matrixing and mobility shift for each set of primers as previously described (42). Briefly, the area under each negative peak was subtracted from that of the corresponding positive peak. The resulting peak area difference at each nt position was divided by the average of the highest 8% of peak area differences, calculated after discounting any results greater than the third quartile plus 1.5× the interquartile range. Normalized intensities were introduced into open-source RNAstructure version 5.7 (48).

Antisense-interfered SHAPE (aiSHAPE)

Locked nucleic acid (LNA)/DNA chimeras were purchased from Exiqon, Woburn, MA, USA the sequences of which are provided in Table 1. Chimeras were added at 10× molar fold excess after folding the RNA. Samples were subsequently incubated at 37°C for 15 min prior to 1M7 treatment (see above). To quantify alterations induced by antisense oligonucleotides, raw data were processed as described above.

3E-5E-GFP minigenome RNA A 3D modeling

The secondary structure of the EBOV 3E-5E-GFP minigenome RNA predicted by RNAstructure software version 5.7 (48) and chemical probing data from SHAPE were used to generate 10 three-dimensional (3D) models for the trailer-to-leader panhandle interaction in the wt EBOV genome and variants, A30U and A26U/A30U, using open-source RNAComposer, version 1.0 (http://rnacomposer.cs.put.poznan.pl/). The quality of predicted models was evaluated using open-source MolProbity and KiNG tools (49,50).

RESULTS

Electrophoretic gel mobility shift assays indicate binding of host-cell proteins to the EBOV trailer

Identification of regions of the EBOV trailer that interact with host proteins was performed by EMSA (Figure 1A) using the primers listed in Table 1. Initially, probes truncated at the 3′ end of the trailer were evaluated to identify host protein binding regions (Supplementary Table). Because each of the larger truncated probes was positive, further EMSAs were performed to define minimal RNA regions of the trailer. Overlapping probes were evaluated in triplicate (Supplementary Table). Background corrected signal intensity was compared to wt and averaged for the replicates. RNP complex formation of probe 1–50 was reduced in the presence of 100× molar fold excess of tRNA with a 35% reduction in binding ($P = 0.024$) indicating that the complex can be competed, but only at high concentrations. No reduction in RNP complex formation was observed when competed with wt, unlabeled probe 1–50 (Figure 1B). The 1–116 probe was significantly competed with unlabeled wt probe at 10×, 25×, 50× and 100×, and 100× tRNA (Figure 1C). The 1–730 probe followed a similar pattern as the 1–116 probe and could be significantly competed with wt unlabeled probe and 50× and 100× tRNA (Figure 1D). The data suggests that the RNP complex formation is specific because low to moderate concentrations of wt competitor and the highest concentrations of tRNA were required for significant competition.

HSPA8 interacts with the 1–116 probe

The 1–116 probe was chosen for use as bait in pull-down assays. Host proteins were eluted from the beads, resolved and analyzed by mass-spectrometry (Figure 2A). *Rattus norvegicus* (peptide score 171.72), *Bos taurus* (peptide score 94.62) and *Mus musculus* (peptide score 370.75) HSPA8 were identified as specifically binding to the 1–116 probe by peptide score and selectivity when compared to the control lane (Figure 2B). Other host proteins binding specifically to the 1–116 probe included ATP5A, mitofilin, aldehyde dehydrogenase and COPS8, but not as consistently or with lower peptide scores (data not shown). IP-RT-PCR confirmed the HSPA8:1-116 interaction (Figure 2C and D). Specific 1–116 probe PCR products were detected only when cell lysates and 1–116 probe were immunoprecipitated with anti-HSPA8 antibody. 1–116 probe could not be detected by PCR in control samples excluding antibody, thus supporting a specific interaction between HSPA8 and the 1–116 probe. Following identification of HSPA8 a literature search was performed indicating that HSPA8 interacts with a pentanucleotide motif, 5′AUUUA3′, (51–54). Closer examination of the EBOV trailer sequence identified three of these motifs at nt positions 26–30, 620–624 and 669–673. Here, these are referred to as HSPA8-binding motifs 1, 2 and 3, respectively.

Mutational analysis of 5′AUUUA HSPA8 motif 1 is necessary for efficient transcription and replication

Based on the EMSA data, HSPA8 motif 1 was chosen for further functional analysis. Variants of motif 1 were generated containing either a single point mutation or clustered multiple point mutations. The effect of these variants on EBOV transcription/replication was examined in the context of the 3E-5E-GFP minigenome assay using 293T cells. The 3E-5E-GFP minigenome assay is a transfection based replicon system in which expression plasmids encoding the EBOV VP30, VP35, L and NP proteins are co-transfected with a plasmid encoding the 3E-5E-GFP minigenome that is driven by a T7 promoter and an expression plasmid encoding the T7 polymerase (T7pol). The minigenome is described in detail in Watanabe *et al.* (10), briefly the 5′ and 3′ ends of the EBOV genome flank a eGFP ORF as a reporter gene and is replication and transcription competent. Single nucleotide changes in motif 1 of the minigenome indicated that an A30U (5′AUUUU3′) mutation resulted in a statistically significant ($P < 0.0001$) decrease in both the total number of GFP-positive cells (47% decrease, Figure 3A)

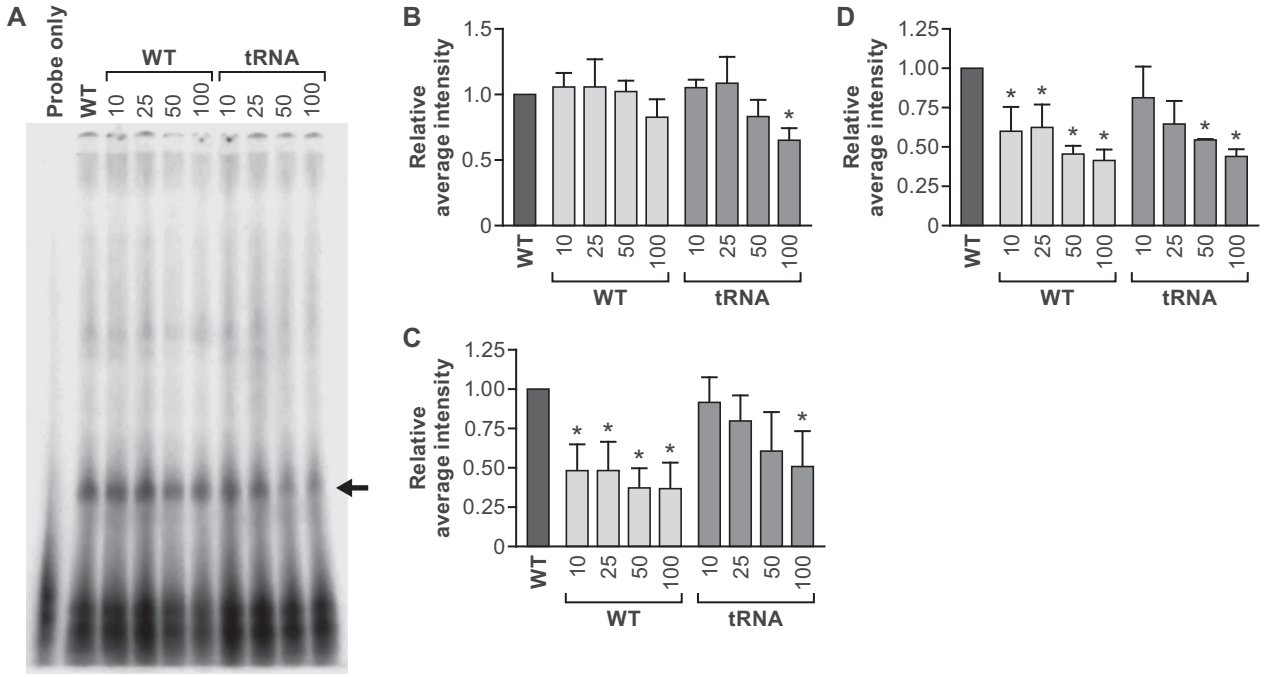

Figure 1. EMSAs of the EBOV trailer demonstrating interaction with host proteins. (**A**) Representative EMSA using probe 1–50 in the presence of cold 1–50 competitor and tRNA. The black arrow indicates the complex used for quantification. (**B**) Relative average background-corrected intensity of at least three independent experiments using the 1–50 probe compared to wt (**C**) Relative quantification of probe 1–116 competition with increasing concentration of unlabeled 1–116. (**D**) Relative quantification of probe 1–730 competition with increasing concentration of unlabeled 1–730. * indicates statistical significance.

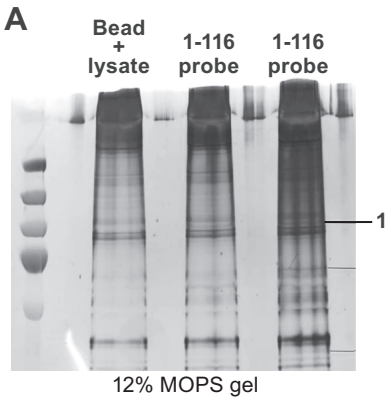

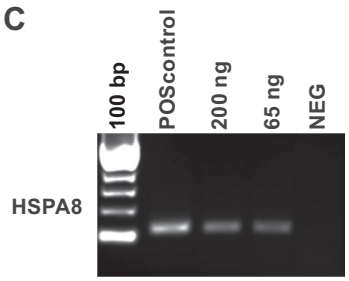

B

Method of selection	Accession	# AAs	ΣCoverage	Description	# Peptides	Score
1-116 probe whole lane	gi178847300	543	15.29	70-Kda heat shock cognate protein from *Rattus norvegicus*	6	171.72
Complete trailer probe	gi28189915	67	58.21	Similar to 70-Kda heat shock cognate protein (*Bos taurus*)	3	94.62
1-116 probe bands	gi74211667	553	35.08	Unnamed protein product (*Mus musculus*) HSPA8	13	370.75

Figure 2. The host protein HSPA8 binds to the EBOV genome trailer. (**A**) Representative silver-stained gel used for mass-spectrometry analysis. Number 1 indicates the area where specific bands were identified)). (**B**) Summation of the mass-spectrometry data identifying HSPA8. (**C**) IP-RT-PCR results confirming interaction between HSPA8 and the EBOV genome trailer. Line labeled as 'NEG' indicates parallel samples that excluded the HSPA8 antibody. (**D**) Western blot confirming immunoprecipitation of HSPA8, NEG indicates parallel control samples that excluded the HSPA8 antibody.

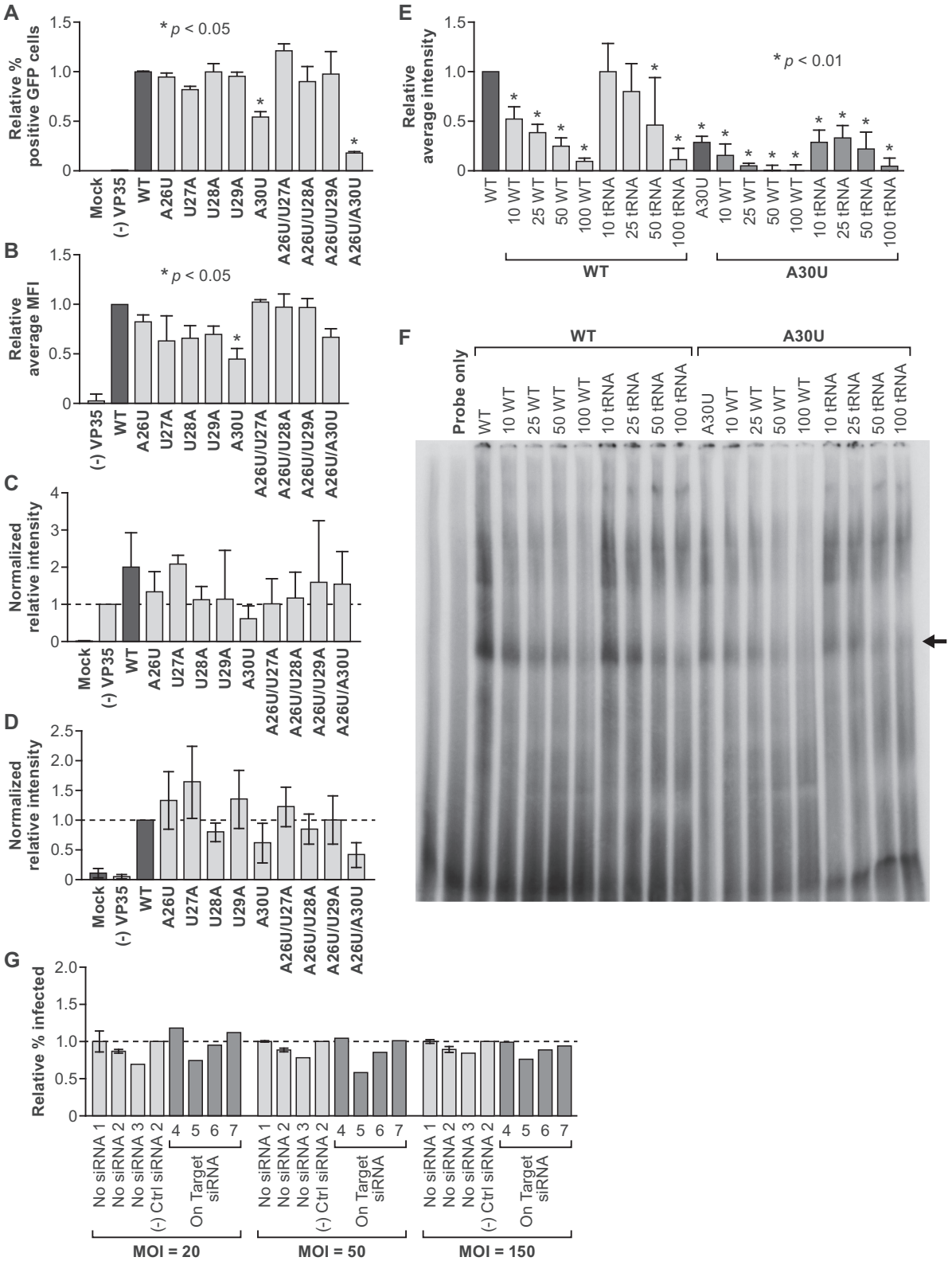

Figure 3. Role of the HSPA8 motif 1 in the EBOV lifecycle. (**A**) Representation of relative percentage of GFP-positive cells transfected with motif 1 single and double mutants. (**B**). Representation of median fluorescence intensity (MFI) for GFP-positive cells infected with motif 1 single and double mutants. (**C**) Northern blot representing the levels of minigenome RNA synthesis for motif 1 mutants (**D**) Northern blot representing the levels of RI synthesis for motif 1 mutants. (**E**). Summary of EMSA data comparing wt 1–116 probe to the HSPA8 motif 1 A30U single nucleotide mutant. (**F**) Representative EMSA. (**G**) siRNA targeting of HSPA8.

and in the mean fluorescence intensity of the GFP signal (43% decrease) (Figure 3B). The A26U/A30U double mutant (5′UUUUU3′) motif resulted in a significant decrease in GFP-positive cells (75%, $P < 0.0001$, Figure 3A and B).

Northern blots specifically targeting the genome and RI RNAs were performed on the wt and mutant minigenome samples to determine which step of the virus lifecycle was impacted by mutagenesis of motif 1. Based on previous identification of VP35 as essential for replication and transcription in an EBOV minigenome assay, (55), a control omitting expression of VP35 (VP35(−)) was included to determine the level of T7pol produced minigenome RNA. This control is necessary to determine the level of minigenome produced by the viral proteins. If the mutant does not impact minigenome synthesis, then the northern blot signal intensity will be increased when compared to VP35(−) and equal to the wt sample. If the mutant impacts minigenome RNA synthesis, then the northern blot signal intensity will be equal to the VP35(−) signal or greater than the wt signal. The data indicate that four of five single point mutations, A26U, U28A, U29A and A30U, in motif 1 reduced minigenome RNA synthesis. The A30U mutant demonstrated the greatest impact and was below the VP35(−) signal (Figure 3C and Supplementary Figure S1A), however the U27A mutant did not impact minigenome RNA synthesis. The double mutants A26U/U27A, A26U/U28A and A26U/A30U also reduced minigenome RNA synthesis when compared to wt. These data indicate that motif 1 is involved in minigenome RNA synthesis.

To assess the impact of motif 1 in RI RNA synthesis, a northern blot specifically targeting the RI RNA was developed (Figure 3D and Supplementary Figure S1B). RI RNA is not produced by T7pol and will only be produced when the appropriate complement of viral proteins and a suitable RNA template is present, therefore the northern blot signal intensity for RI RNA was used as a basis of comparison. Mutants U28A, A30U and A26U/A30U decreased RI RNA synthesis when compared to wt. Mutants A26U, U27A, U29A, A26U/U27A, A26U/U28A and A26U/U29A demonstrated variable but near wt levels of RI RNA synthesis. These data indicate that motif 1 also plays a role in RI RNA synthesis. Interestingly, the VP35(−) control indicates that VP35 is also required for RI RNA synthesis.

Transfection based viral replicons reflect basic viral process, but do not reflect all aspects of the viral lifecycle. Therefore, evaluation of the mutations with the greatest effect in the 3E-5E-eGFP minigenome assay, A30U, A26U/A30U and an additional Δ2–56 mutant, was carried out using a full-length infectious clone (Table 2). The A26U/A30U and Δ2–56 mutants could not be recovered in four of four replicates. However, the A30U EBOV variant was rescued in 3/4 replicates, although with slower kinetics. Sequence analysis of one of three replicates indicated an 'A' insertion at position 6579 in 87% of viral RNAs, which is in the GP open reading frame. As expected, wt EBOV was recovered in all 4 replicates. These data support the importance of motif 1 in the virus lifecycle.

EMSA and siRNA support HSPA8's role in the virus lifecycle

Based on 3E-5E minigenome assay data, the A30U mutant was evaluated for RNP formation by EMSA, using the 1–116 probe. As shown in Figure 3E and F significant competition was observed with cold wt competitor similar to the initial experiments described above. Competition with cold tRNA did not reach significance at 10 or 25× molar concentration, but was observed at 50 and 100× suggesting specificity of the interaction between HSPA8 and the trailer in this probe. EMSA of the 1–116 probe containing the A30U point mutation indicated a 72% decrease in RNP formation ($P < 0.01$, one-way ANOVA Std Dev 0.06) (Figure 3E and F) compared to wt probe. RNP complex formation was competed with both wt and tRNA supporting our hypothesis that A30 of motif 1 is necessary for RNP complex formation ($P < 0.01$ one-way ANOVA, GraphPad Prism).

Chemical modulation and siRNA screening was performed to verify the role of HSPA8 in the virus lifecycle. Cells were pre-treated with oxymatrine, which is used as a HCV inhibitor and modulates HSPA8 mRNA stability (56), but failed clinical trial evaluation (57). Oxymatrine treated cells were infected at an MOI of 3 with EBOV. Oxymatrine treatment of cells minimally reduced viral titer and semi-quantitative western did not support reduction of HSPA8 expression (data not shown). Thus, a previously established siRNA screening assay (43) was used to evaluate four commercially available siRNAs against HSPA8. On-Target siRNA5 reduced relative EBOV infection when compared to No siRNA and negative control siRNA at an MOI 20, 50 and 150 (Figure 3G).

SHAPE indicates that HSPA8 motif 1 forms a stem-loop structure

SHAPE interrogates RNA secondary structure by examining backbone flexibility (directly related to base pairing) at each nucleotide position via reactivity with a specific electrophilic reagent (39). We applied this technique to the EBOV 3E-5E-GFP minigenome RNA, which contains all essential *cis*-acting elements for efficient GFP translation and EBOV minigenome replication *in vitro* (8,10,55).

Reactivity to the SHAPE reagent 1M7 for EBOV minigenome RNA is shown in Figure 4A (Supplementary Figure S2). The most reactive, and thus least structurally constrained residues have a reactivity >0.8. Nucleotide positions with reactivities <0.2 are indicative of fully base paired residues.

Minimum free energy modeling using SHAPE data as pseudo free energy constraints indicated formation of a panhandle duplex structure between trailer and leader (Figure 4A). This long-range RNA–RNA interaction spans the first and last 50 nt of trailer and leader, respectively. The trailer-to-leader panhandle is interrupted by an internal bulge on the leader side (nt 1929–1931) and a three-way junction (nt 22–38 and 1912–1921). The three-way junction embeds a short stem-loop (nt 28–37) containing HSPA8 motif 1.

The region upstream of the leader forms a stem-loop structure (nt 1868–1890) with an AU-rich apical loop, similar to the RI hairpin previously identified as a putative VP30

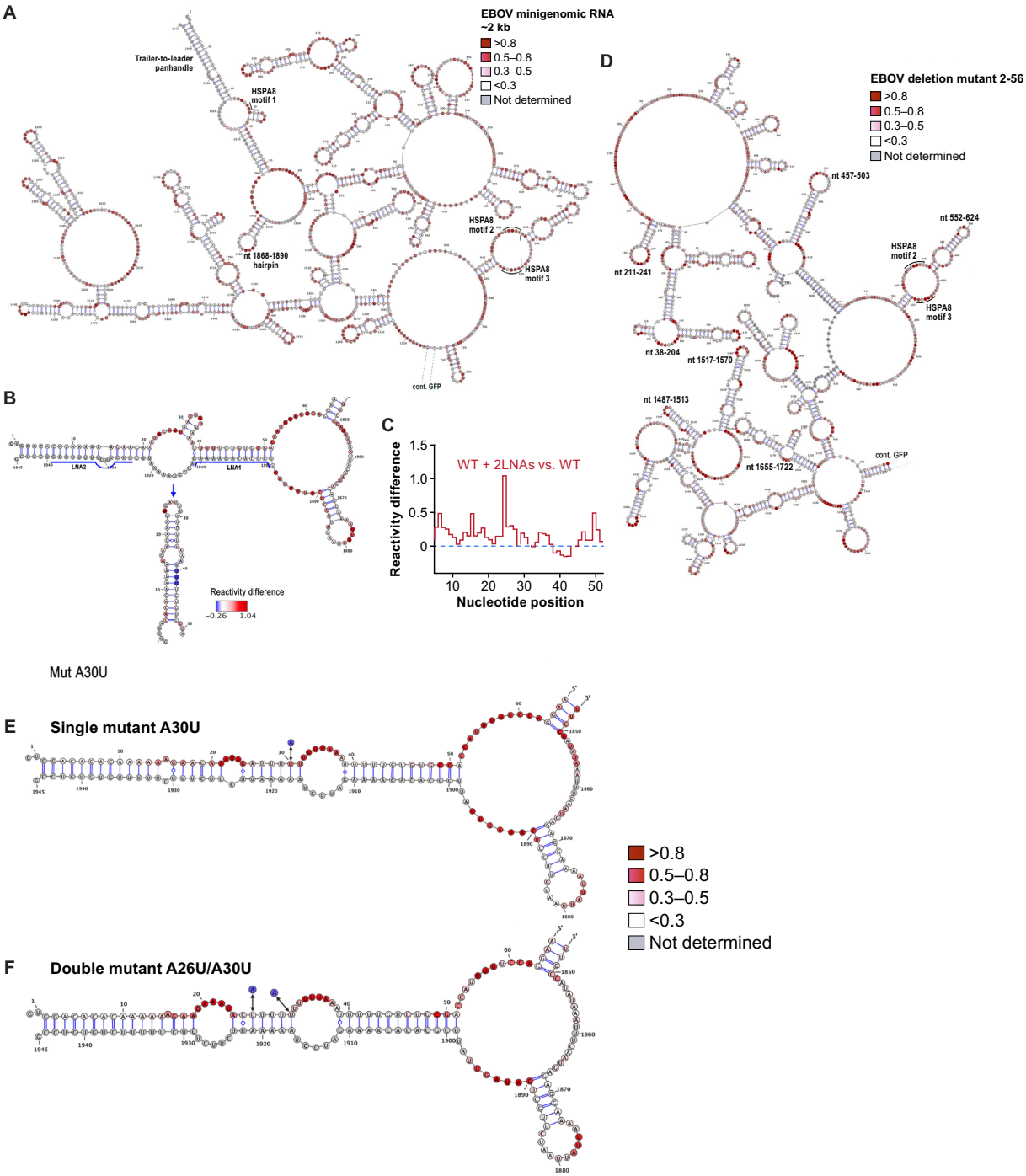

Figure 4. Secondary structure of nt 1–1945 of EBOV 3E-5E minigenome RNA. (**A**) Processed SHAPE reactivities are presented as a function of nucleotide position. Red notations are expected to fall into single-stranded regions, whereas bases indicated in white correspond predominantly to either double-stranded regions or putative tertiary interactions. Gray nucleotides correspond to residues for which no SHAPE signal values were measured either due to pausing during reverse transcription or the position of 3′ primer hybridization. Data shown are an average of at least three experiments. Individual RNA domains have been annotated trailer-to-leader interaction, HSPA8 motifs 1–3 and the nt 1868–1890 hairpin. * cont. GFP indicates a break in the structure which contains the GFP open reading frame. (**B**) Structural response of the trailer-to-leader panhandle to antisense oligomers. The secondary structure of the wt EBOV minigenome RNA is indicated according to SHAPE predictions. Gray residues represent formation of an extensive stop during reverse transcription at the position of LNA hybridization. The position of two LNA/DNA chimeras hybridized to the leader is indicated with blue lines. RNAstructure predicted alteration of the trailer structure is indicated below. Residues resulting in a reactivity increase (red) or decrease (blue) are indicated. (**C**) Step plot representing the reactivity difference noted within nt 1–50 of the trailer in SHAPE and aiSHAPE experiments. (**D**) Structural map of the Δ2–56 EBOV minigenome RNA mutant**.** Domains unaffected by introducing the deletion as compared to wt EBOV are indicated. Nucleotide reactivities are color-coded as shown in the key and numbered every 10 nt. * cont. GFP indicates a break in the structure which contains the GFP open reading frame. (**E** and **F**) Structural map of the trailer-to-leader interaction for the A30U and A26UA30U mutants, respectively. Sites of mutation are indicated with arrows.

Table 2. Infectious EBOV clone rescue results

Experiment	Replicate	A30U	A26UA30U	Δ2–56 deletion
Experiment 1	Replicate 1	Not recovered	Not recovered	Not recovered
	Replicate 2	100% infectivity at passage 2 (Insertion of A at nt 6579)	Not recovered	Not recovered
Experiment 2	Replicate 1	63% infectivity at passage 2	Not recovered	Not recovered
	Replicate 2	42% infectivity at passage 2	Not recovered	Not recovered

binding site (14). Residues A1874–U1879 of this hairpin reacted more strongly with 1M7 than residues U1880–U1883. Thus, the possibility exists that this hairpin (nt 1879–1884) forms an H-type pseudoknot structure with the 5′ upstream complementary region (nt 1863–1868). Pseudoknots play a critical role in many biological activities, from regulation of viral gene expression to catalysis of mRNA splicing and repeat-addition processivity of human telomerase (58,59). Subsequent experiments involving LNA-directed displacement of the putative pseudoknot interaction (aiSHAPE) (40) did not change reactivity of apical loop residues or flanking regions (data not shown). Conceivably, weaker reactivities of the apical loop of this hairpin can be attributed to intraloop base-stacking interaction between AU residues.

HSPA8 motifs 2 (nt 620–624) and 3 (nt 669–673) are located in an unstructured single-stranded region forming the internal loop (nt 612–625, nt 662–674) of a hairpin preceding the GFP sequence (Figure 4A). Importantly, the GFP sequence base pairs independently (Supplementary Figure S2).

aiSHAPE data substantiate the EBOV trailer-to-leader panhandle interaction

To validate the trailer-to-leader interaction, we applied aiSHAPE (40). Experimentally, one strand of an RNA duplex is displaced by hybridizing an antisense DNA/LNA oligonucleotide, and disrupted RNA–RNA interactions are characterized by enhanced 1M7 reactivity of the displaced nucleotides.

Two chimeric LNA/DNA oligonucleotides, 3′-LNA1 and 3′-LNA2 (Table 1) were hybridized to the leader (nt 1889–1911 and nt 1925–1939) to disrupt base pairing interaction with the trailer (wt + 2LNAs). In the control sample, these oligonucleotides were omitted (wt). aiSHAPE indicated changes in chemical reactivity within trailer residues (Figure 4B). In particular, nts C5–A37 and U43–A51 of the experimental sample (wt + 2LNAs) were more sensitive to 1M7 modification (median reactivity 0.49) than the corresponding residues in the control sample (wt, median reactivity of 0.27). Moreover, nts A38–U42 of wt + 2LNAs were less reactive (median value 0.39) than their wt counterparts (median value 0.54). The RNAstructure algorithm, when provided with pseudo energy constraints retrieved from aiSHAPE experiments, predicted that in the absence of its interacting 3′ partner, the trailer forms an independent stem-loop structure involving nts C5–G48 (Figure 4B). The stem of this hairpin is mainly composed of A:U base pairs, interrupted by only two G:C pairs and one G:U wobble.

The specificity of the aiSHAPE strategy was verified by formation of an extensive barrier to reverse transcription at the sites of LNA/DNA hybridization, as revealed during capillary electrophoresis separation of the reverse transcription products (data not shown). The 1M7 reactivity profile in the presence of both LNAs indicated minor off-site changes, which could reflect perturbation of tertiary contacts within EBOV minigenome RNA (Supplementary Figure S3).

Mutating the EBOV trailer affects the structural conformation of the trailer-to-leader panhandle structure

We performed structural analysis of EBOV minigenome RNA mutants Δ2–56, A30U and A26U/A30U to address how changes introduced within the trailer affect the conformation of the trailer-to-leader panhandle. Although the lack of trailer sequence induced structural rearrangements in deletion mutant Δ2–56 (Figure 4D; Supplementary Figures S4 and 5), certain structural domains specific for wt EBOV minigenome RNA remained unchanged. These include a bifurcated stem-loop at the 5′ terminus (nts 38–204), a stem-loop occluding HSPA8 motifs 2 and 3 (nts 552–624) and the hairpin structure previously proposed as VP30-binding site (nts 1813–1835) (Figure 4D). In contrast, the A30U mutation within motif 1 affected only the conformation of the trailer-to-leader panhandle (Figure 4E and Supplementary Figure S6). This single nucleotide substitution eliminated formation of the nt 28–37 hairpin (containing HSPA8 motif 1 in wt RNA), and introduced an A:C mispair (nt A15, C1931) and an asymmetric internal loop (nt 22–24 and 1925) (Figure 4E). Similarly, the A26U/A30U point mutations caused structural rearrangements of the panhandle duplex, again eliminating the nt 28–37 stem-loop and introducing a mismatch at position 15 and an additional internal loop (G19–U23 and C1924–U1928) (Figure 4F and Supplementary Figure S7).

Three-dimensional modeling of the EBOV minigenome trailer-to-leader panhandle structure

A 3D structural model of the EBOV trailer and leader was generated using RNAComposer (60) (Figure 5). Since the server does not accept sequences >500 nts, a 174-nt derivative sequence was created by deleting the sequences downstream of nt 66 and upstream of nt 1847 and closing the remaining short helical region (G63–A66 and U1847–C1850) with a -G-A-G-A tetraloop. A dot-bracket notation generated by RNAstructure software was manually adjusted to account for this deletion, and subsequently provided to RNAComposer. Ten 3D RNA models were generated and analyzed, taking into account their secondary structure topology, sequence homology, structure resolution and free energy. In addition, the quality of predicted

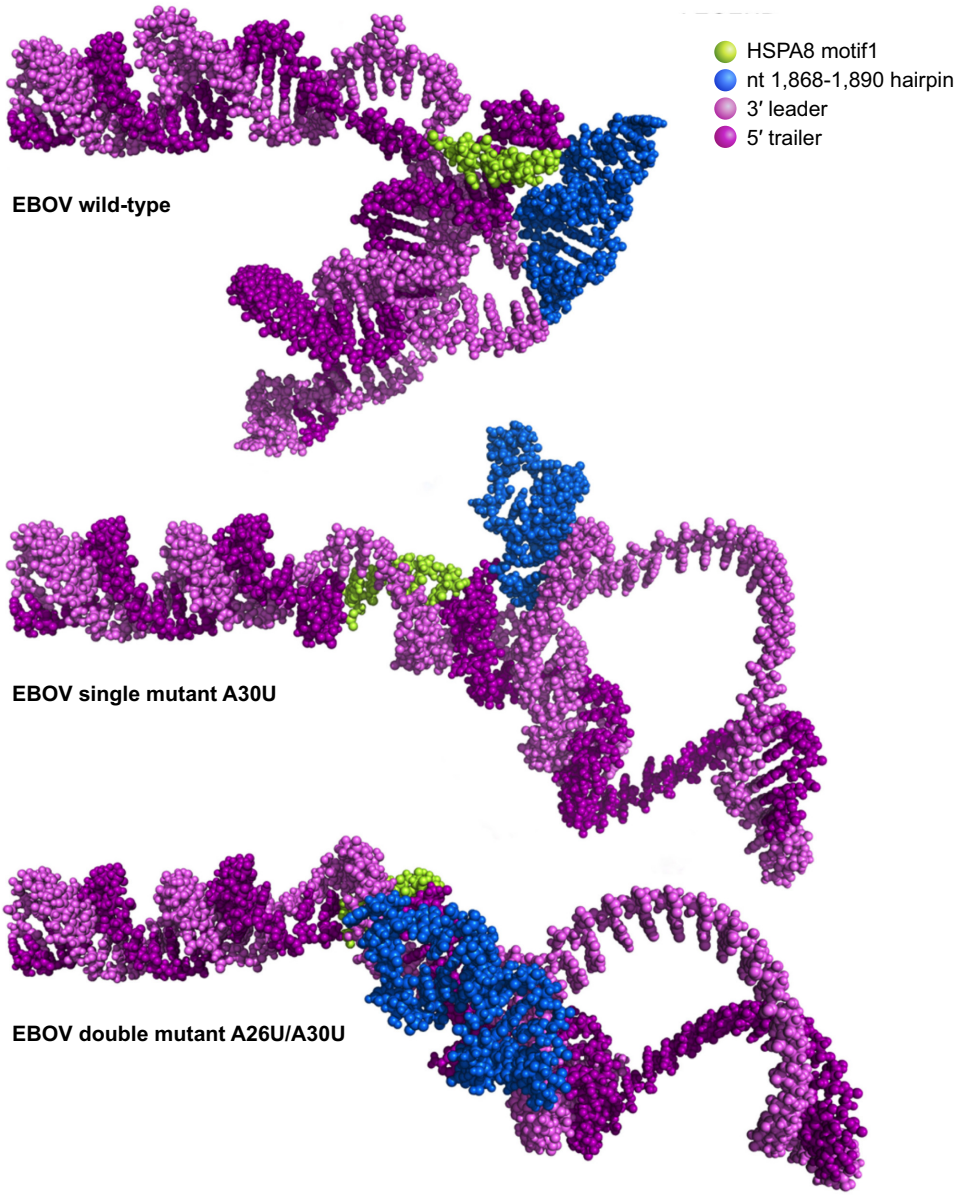

Figure 5. Three-dimensional projection models of the trailer-to-leader interaction in EBOV minigenome wt, A30U and A26UA30U RNAs. The 170 nt of internally deleted EBOV minigenome RNA are depicted. Specific *cis*-acting motifs and domains are color-coded as shown in the key. The models indicate that the previously defined VP30-binding site stem-loop is near to HSPA8 motif 1. A30U and A26UA30U mutations affect the spatial arrangement between these stem-loop structures.

models was evaluated using MolProbity (4.3) and KiNG tools (49,50). The models with the best topological score are presented in Figure 5, indicating the position of trailer, leader, HSPA8 motif 1 and the nt 1868–1890 hairpin. The wt model reveals close spatial arrangement of HSPA8 motif 1 (green) with the hairpin (blue). The presence of trailer A30U and A26U/A30U mutations changed the distance between these RNA motifs. The model presented here provides useful insight into how RNA substructures may interact during the course of EBOV replication.

DISCUSSION

Accumulation of viral proteins during infections often leads to cellular stress and upregulation of HSP expression (61). The role of HSPs in the viral lifecycle is only just being unveiled (62–64). Numerous studies also indicate that specific interactions of host proteins with viral secondary and tertiary RNA motifs modulate the lifecycle (65,66). In this manuscript, we provide novel insight into the structural conformation of EBOV NCRs, identify a specific RNA motif within the trailer that interacts with a host cell chaperone, HSPA8 and define the role of this protein/RNA interaction in viral replication.

EMSA (Figure 1), followed by protein pull-downs, mass spectrometry and IP-RT-PCR (Figure 2) allowed us to identify and confirm that HSPA8 interacts with the first 50 nts of the EBOV trailer region. HSPA8, a member of the HSC70 family, is a host chaperone that assists mis-folded polypeptide chains to (re)fold into functional proteins and is crucial for cell survival during stress (60). HSC70 also interacts with HCV particles, HSC70 downregulation significantly reduced virus production either via modulation of viral assembly or release (61). In addition, HSC70 was shown to be part of a protein complex that includes HCV NS5A and host proteins HSP70 and HSP40 (62) and was demonstrated to assist the NS5A/HSP70 complex essential for HCV IRES-mediated translation. HSC70 is also recruited to reovirus viral factories (63), and is present in influenza A virus (64), and vesicular stomatitis Indiana virus viral particles (65).

The pentanucleotide motif 5′AUUUA3′ is an HSPA8-interacting motif (51–54). Sequence analysis of the 3E-5E-GFP minigenomic RNA suggested three putative HSPA8 motifs in the trailer. However, the exact structural conformation of these regions was undefined. Thus, using chemical acylation techniques and site-directed mutagenesis, we determined the secondary structure of 3E-5E-GFP EBOV minigenome RNA and demonstrated that its 5′ and 3′ NCRs forms complex long-range RNA interaction including a trailer-to-leader panhandle (Figure 4A and Supplementary Figure S2). Closer analysis indicates that motif 1 forms part of a small stem-loop (nts 28–37) that is in near proximity to the VP30 binding stem loop (nts 1868–1890). To further investigate the role of the 5′ terminal 50 nt in the 5′–3′ interaction and the importance of HSPA8 motif 1, a deletion mutant (Δ2–56) was evaluated by chemical probing and in the context of an EBOV infectious clone. SHAPE data indicate that deleting trailer sequences caused structural changes within the 3E-5E-GFP minigenome RNA, mainly due to the release of the leader sequences for base pairing with complementary regions (Figure 4D; Supplementary Figures S4 and 5). These structural rearrangements did not affect the topology of other RNA domains. Experiments with the infectious clone system indicated that EBOV mutant Δ2–56 was not viable (Table 2). Since HSPA8 motif 1 is located within the 5′ terminal 50 nts of the trailer, it is difficult to unambiguously determine if the panhandle structure or the HSPA8 motif 1 is necessary for virus growth, but such data do reinforce the importance of HSPA8 motif 1.

Probing analysis of the A30U and A26U/A30U minigenome RNAs showed that HSPA8 motif 1 point mutations affect the panhandle conformation, eliminating the nt 28–37 stem-loop containing HSPA8 motif 1 (Figure 4E and F). No other RNA domains outside of the 5′–3′ interaction were changed (Supplementary Figures S6 and 7), suggesting the trailer-to-leader interaction forms an independent structural/regulatory element essential for efficient virus replication. Hybridization of LNA/DNA chimeras to the leader did not induce extensive structural changes within upstream domains suggests that the trailer-to-leader panhandle might indeed function as an autonomous element (Supplementary Figure S3). The infectious clone system experiments also indicated that EBOV mutant A26U/A30U was not viable. On the other hand, the A30U mutant was rescued but with slower kinetics. Sequence analysis indicated an A insertion into the the GP open reading frame in 87% of the viral RNAs at position 6579. The effect of this insertion, if any, on viral replication remains to be determined (Table 2).

Automated 3D structure modeling of the trailer-to-leader interaction in the wt 3E-5E-GFP minigenome RNA implied a close association of HSPA8 motif 1 with the 1868–1890 hairpin, recently shown to bind VP30 (18) (Figure 5). The first 21 nt of the interacting 5′-3′ regions form an extended arm that is positioned orthogonally to the interacting HSPA8/1868–1890 motifs. The spatial proximity of these elements suggests a potential molecular bridging between HSPA8/VP30 and their specific RNA-binding motifs. A30U and A26U/A30U mutations changed the spatial arrangement between these stem-loop structures possibly disrupting these complex long-range interactions (Figure 5).

Mutational analysis of HSPA8 motif 1 further confirmed its importance in the EBOV lifecycle (Figure 3A and B). In particular, single and double point mutations indicated that residue A30 plays an essential role in viral replication and transcription. Furthermore, northern blot data indicated a reduction in both minigenome and RI RNA production for the A30U mutant (Figure 3D and Supplementary Figure S1). The A26U/A30U double mutation also resulted in reduced RI RNA and minigenome synthesis. Since the RI RNA serves a template for synthesis of the minigenome RNA, reduction in minigenome RNA most likely directly affects production of RI RNA. In addition, EMSA analysis of the A30U mutant demonstrated reduced host protein/viral RNA/RNP complex formation (Figure 3E). It is interesting that siRNA-directed (Figure 3G) or chemical inhibition (data not shown) of HSPA8 moderately reduced infectivity and viral titer, respectively, whereas EBOV genome mutagenesis that targets the HSPA8 binding motif led to nonviable virus.

Taken together, our structural probing, mutagenesis and reverse genetics data indicate that the conformation of the EBOV trailer and its interactions with host cell HSPA8 are essential regulators of the EBOV lifecycle. Our studies indicate that HSPA8 plays a critical role in production of viral genomic and RI RNAs. During transcription and replication, the viral genome must become a template for synthesis of progeny RNA. This process involves uncoating or at least relaxation of the viral RNP. Host factors likely interact with the viral RNP to maintain proximity of necessary factors and aid complex formation to initiate and complete these processes (67–69). It is likely that many of these interactions are weak and transient, acting as scaffolds for virus-driven processes. These transient interactions may assist proper RNA folding for RI RNA synthesis, transcription complex formation or proper confirmation of packaging signals to drive discrimination by viral components to ensure effective packaging of full-length genomes and reduction of defective particles.

SUPPLEMENTARY DATA

Supplementary Data are available at NAR Online.

ACKNOWLEDGMENTS

We are grateful to Peter B. Jahrling, Jennifer Sword, Cindy Allan, Krisztina B. Janosko, Stacy L. Agar, Richard Bennett, Michael R. Holbrook and the entire EVPS and IRF-Frederick team for their support and fruitful discussions about these experiments. We thank Dr John L. Casey and Brittany L. Griffin for their discussions about SHAPE. We thank Dr Y. Kawaoka, University of Wisconsin for the EBOV 3E-5E eGFP minigenome system. We thank Laura Bollinger and Jiro Wada for editing the manuscript and for preparing figures, respectively. The content of this publication does not necessarily reflect the views or policies of the US Department of the Army, the US Department of Defense, US Department of Health and Human Services (DHHS) or of the institutions and companies affiliated with the authors

FUNDING

NIAID Division of Intramural Research; Intramural Research Program of the National Cancer Institute (to S.L.G., J.S.-S.); National Institutes of Health, Department of Health and Human Services; Battelle Memorial Institute's prime contract with the US National Institute of Allergy and Infectious Diseases (NIAID) [HHSN272200700016I, in part]; Battelle Memorial Institute (to J.H.K.); Joint Science and Technology Office for Chemical and Biological Defense (JSTO-CBD) of the Defense Threat Reduction Agency (DTRA) [1323839, CCAR# CB3849 to S.R.R.]; Defense Threat Reduction Agency [CB10217 to S.R.R., L.J., in part]. Funding for open access charge: NIH; NIAID; Division of Intramural Research.

Conflict of interest statement. None declared.

REFERENCES

1. Elliott,L.H., Sanchez,A., Holloway,B.P., Kiley,M.P. and McCormick,J.B. (1993) Ebola protein analyses for the determination of genetic organization. *Arch. Virol.*, **133**, 423–436.
2. Sanchez,A., Kiley,M.P., Holloway,B.P. and Auperin,D.D. (1993) Sequence analysis of the Ebola virus genome: organization, genetic elements, and comparison with the genome of Marburg virus. *Virus Res.*, **29**, 215–240.
3. Brauburger,K., Boehmann,Y., Tsuda,Y., Hoenen,T., Olejnik,J., Schumann,M., Ebihara,H. and Muhlberger,E. (2014) Analysis of the highly diverse gene borders in Ebola virus reveals a distinct mechanism of transcriptional regulation. *J. Virol.*, **88**, 12558–12571.
4. Fricke,M., Dunnes,N., Zayas,M., Bartenschlager,R., Niepmann,M. and Marz,M. (2015) Conserved RNA secondary structures and long-range interactions in hepatitis C viruses. *RNA*, **21**, 1219–1232.
5. Mauger,D.M., Siegfried,N.A. and Weeks,K.M. (2013) The genetic code as expressed through relationships between mRNA structure and protein function. *FEBS Lett.*, **587**, 1180–1188.
6. Thurner,C., Witwer,C., Hofacker,I.L. and Stadler,P.F. (2004) Conserved RNA secondary structures in Flaviviridae genomes. *J. Gen. Virol.*, **85**, 1113–1124.
7. Yang,D. and Leibowitz,J.L. (2015) The structure and functions of coronavirus genomic 3′ and 5′ ends. *Virus Res.*, **206**, 120–133.
8. Muhlberger,E., Weik,M., Volchkov,V.E., Klenk,H.D. and Becker,S. (1999) Comparison of the transcription and replication strategies of marburg virus and Ebola virus by using artificial replication systems. *J. Virol.*, **73**, 2333–2342.
9. Muhlberger,E., Trommer,S., Funke,C., Volchkov,V., Klenk,H.D. and Becker,S. (1996) Termini of all mRNA species of Marburg virus: sequence and secondary structure. *Virology*, **223**, 376–380.
10. Watanabe,S., Watanabe,T., Noda,T., Takada,A., Feldmann,H., Jasenosky,L.D. and Kawaoka,Y. (2004) Production of novel ebola virus-like particles from cDNAs: an alternative to ebola virus generation by reverse genetics. *J. Virol.*, **78**, 999–1005.
11. Uebelhoer,L.S., Albarino,C.G., McMullan,L.K., Chakrabarti,A.K., Vincent,J.P., Nichol,S.T. and Towner,J.S. (2014) High-throughput, luciferase-based reverse genetics systems for identifying inhibitors of Marburg and Ebola viruses. *Antiviral Res.*, **106**, 86–94.
12. Volchkov,V.E., Volchkova,V.A., Chepurnov,A.A., Blinov,V.M., Dolnik,O., Netesov,S.V. and Feldmann,H. (1999) Characterization of the L gene and 5′ trailer region of Ebola virus. *J. Gen. Virol.*, **80**, 355–362.
13. Crary,S.M., Towner,J.S., Honig,J.E., Shoemaker,T.R. and Nichol,S.T. (2003) Analysis of the role of predicted RNA secondary structures in Ebola virus replication. *Virology*, **306**, 210–218.
14. Weik,M., Modrof,J., Klenk,H.D., Becker,S. and Muhlberger,E. (2002) Ebola virus VP30-mediated transcription is regulated by RNA secondary structure formation. *J. Virol.*, **76**, 8532–8539.
15. Weik,M., Enterlein,S., Schlenz,K. and Muhlberger,E. (2005) The Ebola virus genomic replication promoter is bipartite and follows the rule of six. *J. Virol.*, **79**, 10660–10671.
16. Biedenkopf,N., Lier,C. and Becker,S. (2016) Dynamic phosphorylation of VP30 is essential for Ebola virus life cycle. *J. Virol.*, **90**, 4914–4925.
17. Biedenkopf,N., Schlereth,J., Grunweller,A., Becker,S. and Hartmann,R.K. (2016) RNA binding of Ebola virus VP30 is essential for activating viral transcription. *J. Virol.*, **90**, 7481–7496.
18. Schlereth,J., Grunweller,A., Biedenkopf,N., Becker,S. and Hartmann,R.K. (2016) RNA binding specificity of Ebola virus transcription factor VP30. *RNA Biol.*, 1–16.
19. Mehedi,M., Hoenen,T., Robertson,S., Ricklefs,S., Dolan,M.A., Taylor,T., Falzarano,D., Ebihara,H., Porcella,S.F. and Feldmann,H. (2013) Ebola virus RNA editing depends on the primary editing site sequence and an upstream secondary structure. *PLoS Pathog.*, **9**, e1003677.
20. Sanchez,A., Trappier,S.G., Mahy,B.W., Peters,C.J. and Nichol,S.T. (1996) The virion glycoproteins of Ebola viruses are encoded in two reading frames and are expressed through transcriptional editing. *Proc. Natl. Acad. Sci. U.S.A.*, **93**, 3602–3607.
21. Volchkov,V.E., Becker,S., Volchkova,V.A., Ternovoj,V.A., Kotov,A.N., Netesov,S.V. and Klenk,H.D. (1995) GP mRNA of Ebola virus is edited by the Ebola virus polymerase and by T7 and vaccinia virus polymerases. *Virology*, **214**, 421–430.
22. Shwetha,S., Kumar,A., Mullick,R., Vasudevan,D., Mukherjee,N. and Das,S. (2015) HuR displaces polypyrimidine tract binding protein to facilitate la binding to the 3′ untranslated region and enhances Hepatitis C virus replication. *J. Virol.*, **89**, 11356–11371.
23. Kanda,T., Gauss-Muller,V., Cordes,S., Tamura,R., Okitsu,K., Shuang,W., Nakamoto,S., Fujiwara,K., Imazeki,F. and Yokosuka,O. (2010) Hepatitis A virus (HAV) proteinase 3C inhibits HAV IRES-dependent translation and cleaves the polypyrimidine tract-binding protein. *J. Viral Hepat.*, **17**, 618–623.
24. Walter,B.L., Nguyen,J.H., Ehrenfeld,E. and Semler,B.L. (1999) Differential utilization of poly(rC) binding protein 2 in translation directed by picornavirus IRES elements. *RNA*, **5**, 1570–1585.
25. Phillips,S.L., Soderblom,E.J., Bradrick,S.S. and Garcia-Blanco,M.A. (2016) Identification of proteins bound to dengue viral RNA in vivo reveals new host proteins important for virus replication. *Mbio*, **7**.
26. Spagnolo,J.F. and Hogue,B.G. (2000) Host protein interactions with the 3′ end of bovine coronavirus RNA and the requirement of the poly(A) tail for coronavirus defective genome replication. *J. Virol.*, **74**, 5053–5065.
27. Shen,X. and Masters,P.S. (2001) Evaluation of the role of heterogeneous nuclear ribonucleoprotein A1 as a host factor in murine coronavirus discontinuous transcription and genome replication. *Proc. Natl. Acad. Sci. U.S.A.*, **98**, 2717–2722.
28. Johnson,R.F., Feng,M., Liu,P., Millership,J.J., Yount,B., Baric,R.S. and Leibowitz,J.L. (2005) Effect of mutations in the mouse hepatitis virus 3′(+)42 protein binding element on RNA replication. *J. Virol.*, **79**, 14570–14585.
29. Nanda,S.K. and Leibowitz,J.L. (2001) Mitochondrial aconitase binds to the 3′ untranslated region of the mouse hepatitis virus genome. *J. Virol.*, **75**, 3352–3362.

30. Kurilla,M.G., Cabradilla,C.D., Holloway,B.P. and Keene,J.D. (1984) Nucleotide sequence and host La protein interactions of rabies virus leader RNA. *J. Virol.*, **50**, 773–778.
31. Wilusz,J., Kurilla,M.G. and Keene,J.D. (1983) A host protein (La) binds to a unique species of minus-sense leader RNA during replication of vesicular stomatitis virus. *Proc. Natl. Acad. Sci. U.S.A.*, **80**, 5827–5831.
32. Raha,T., Pudi,R., Das,S. and Shaila,M.S. (2004) Leader RNA of Rinderpest virus binds specifically with cellular La protein: a possible role in virus replication. *Virus Res.*, **104**, 101–109.
33. Takahashi,K., Halfmann,P., Oyama,M., Kozuka-Hata,H., Noda,T. and Kawaoka,Y. (2013) DNA topoisomerase 1 facilitates the transcription and replication of the Ebola virus genome. *J. Virol.*, **87**, 8862–8869.
34. Jardine,D., Tachedjian,G., Locarnini,S. and Birch,C. (1993) Cellular topoisomerase I activity associated with HIV-1. *AIDS Res. Hum. Retroviruses*, **9**, 1245–1250.
35. Takahashi,H., Tatsumi,M., Matsuda,M., Nagashima,K., Kurata,T. and Hall,W.W. (1997) The role of topoisomerase I in HIV-1 replication. *Leukemia*, **11(Suppl. 3)**, 113–115.
36. Takahashi,H., Sawa,H., Hasegawa,H., Shoya,Y., Sata,T., Hall,W.W., Nagashima,K. and Kurata,T. (2002) Topoisomerase I and ATP activate cDNA synthesis of human immunodeficiency virus type 1. *Biochem. Biophys. Res. Commun.*, **294**, 509–517.
37. Champoux,J.J. (2001) DNA topoisomerases: structure, function, and mechanism. *Annu. Rev. Biochem.*, **70**, 369–413.
38. Merino,E.J., Wilkinson,K.A., Coughlan,J.L. and Weeks,K.M. (2005) RNA structure analysis at single nucleotide resolution by selective 2′-hydroxyl acylation and primer extension (SHAPE). *J. Am. Chem. Soc.*, **127**, 4223–4231.
39. Wilkinson,K.A., Merino,E.J. and Weeks,K.M. (2006) Selective 2′-hydroxyl acylation analyzed by primer extension (SHAPE): quantitative RNA structure analysis at single nucleotide resolution. *Nat. Protoc.*, **1**, 1610–1616.
40. Legiewicz,M., Zolotukhin,A.S., Pilkington,G.R., Purzycka,K.J., Mitchell,M., Uranishi,H., Bear,J., Pavlakis,G.N., Le Grice,S.F. and Felber,B.K. (2010) The RNA transport element of the murine musD retrotransposon requires long-range intramolecular interactions for function. *J. Biol. Chem.*, **285**, 42097–42104.
41. Johnson,R.F., McCarthy,S.E., Godlewski,P.J. and Harty,R.N. (2006) Ebola virus VP35-VP40 interaction is sufficient for packaging 3E-5E minigenome RNA into virus-like particles. *J. Virol.*, **80**, 5135–5144.
42. Vasa,S.M., Guex,N., Wilkinson,K.A., Weeks,K.M. and Giddings,M.C. (2008) ShapeFinder: a software system for high-throughput quantitative analysis of nucleic acid reactivity information resolved by capillary electrophoresis. *RNA*, **14**, 1979–1990.
43. Radoshitzky,S.R., Pegoraro,G., Chi,X.O., L,D.N., Chiang,C.Y., Jozwick,L., Clester,J.C., Cooper,C.L., Courier,D., Langan,D.P. *et al.* (2016) siRNA screen identifies trafficking host factors that modulate alphavirus infection. *PLoS Pathog.*, **12**, e1005466.
44. Radoshitzky,S.R., Dong,L., Chi,X., Clester,J.C., Retterer,C., Spurgers,K., Kuhn,J.H., Sandwick,S., Ruthel,G., Kota,K. *et al.* (2010) Infectious Lassa virus, but not filoviruses, is restricted by BST-2/tetherin. *J. Virol.*, **84**, 10569–10580.
45. Mate,S.E., Kugelman,J.R., Nyenswah,T.G., Ladner,J.T., Wiley,M.R., Cordier-Lassalle,T., Christie,A., Schroth,G.P., Gross,S.M., Davies-Wayne,G.J. *et al.* (2015) Molecular evidence of sexual transmission of Ebola virus. *N. Engl. J. Med.*, **373**, 2448–2454.
46. Steen,K.A., Siegfried,N.A. and Weeks,K.M. (2011) Selective 2′-hydroxyl acylation analyzed by protection from exoribonuclease (RNase-detected SHAPE) for direct analysis of covalent adducts and of nucleotide flexibility in RNA. *Nat. Protoc.*, **6**, 1683–1694.
47. Mitra,S., Shcherbakova,I.V., Altman,R.B., Brenowitz,M. and Laederach,A. (2008) High-throughput single-nucleotide structural mapping by capillary automated footprinting analysis. *Nucleic Acids Res.*, **36**, e63.
48. Reuter,J.S. and Mathews,D.H. (2010) RNAstructure: software for RNA secondary structure prediction and analysis. *BMC Bioinformatics*, **11**, 129.
49. Chen,V.B., Arendall,W.B. 3rd, Headd,J.J., Keedy,D.A., Immormino,R.M., Kapral,G.J., Murray,L.W., Richardson,J.S. and Richardson,D.C. (2010) MolProbity: all-atom structure validation for macromolecular crystallography. *Acta Crystallogr. D Biol. Crystallogr.*, **66**, 12–21.
50. Chen,Q. and Chen,Y.P. (2011) Modeling conserved structure patterns for functional noncoding RNA. *IEEE Trans. Biomed. Eng.*, **58**, 1528–1533.
51. Henics,T., Nagy,E., Oh,H.J., Csermely,P., von Gabain,A. and Subjeck,J.R. (1999) Mammalian Hsp70 and Hsp110 proteins bind to RNA motifs involved in mRNA stability. *J. Biol. Chem.*, **274**, 17318–17324.
52. Matsui,H., Asou,H. and Inaba,T. (2007) Cytokines direct the regulation of Bim mRNA stability by heat-shock cognate protein 70. *Mol. Cell*, **25**, 99–112.
53. Wilson,G.M., Sutphen,K., Bolikal,S., Chuang,K.Y. and Brewer,G. (2001) Thermodynamics and kinetics of Hsp70 association with A + U-rich mRNA-destabilizing sequences. *J. Biol. Chem.*, **276**, 44450–44456.
54. Zimmer,C., von Gabain,A. and Henics,T. (2001) Analysis of sequence-specific binding of RNA to Hsp70 and its various homologs indicates the involvement of N- and C-terminal interactions. *RNA*, **7**, 1628–1637.
55. Muhlberger,E., Lotfering,B., Klenk,H.D. and Becker,S. (1998) Three of the four nucleocapsid proteins of Marburg virus, NP, VP35, and L, are sufficient to mediate replication and transcription of Marburg virus-specific monocistronic minigenomes. *J. Virol.*, **72**, 8756–8764.
56. Wang,Y.P., Liu,F., He,H.W., Han,Y.X., Peng,Z.G., Li,B.W., You,X.F., Song,D.Q., Li,Z.R., Yu,L.Y. *et al.* (2010) Heat stress cognate 70 host protein as a potential drug target against drug resistance in hepatitis B virus. *Antimicrob. Agents Chemother.*, **54**, 2070–2077.
57. Liu,J., Manheimer,E., Tsutani,K. and Gluud,C. (2003) Medicinal herbs for hepatitis C virus infection: a Cochrane hepatobiliary systematic review of randomized trials. *Am. J. Gastroenterol.*, **98**, 538–544.
58. Staple,DW and Butcher,SE (2005) Pseudoknots: RNA structures with diverse functions. *PLoS Biol.*, **3**.
59. Moon,J.S., Lee,S.H., Kim,E.J., Cho,H., Lee,W., Kim,G.W., Park,H.J., Cho,S.W., Lee,C. and Oh,J.W. (2016) Inhibition of Hepatitis C virus in mice by a small interfering RNA targeting a highly conserved sequence in viral IRES pseudoknot. *PLoS One*, **11**, e0146710.
60. Popenda,M., Szachniuk,M., Antczak,M., Purzycka,K.J., Lukasiak,P., Bartol,N., Blazewicz,J. and Adamiak,R.W. (2012) Automated 3D structure composition for large RNAs. *Nucleic Acids Res.*, **40**, e112.
61. Pastorino,B., Boucomont-Chapeaublanc,E., Peyrefitte,C.N., Belghazi,M., Fusai,T., Rogier,C., Tolou,H.J. and Almeras,L. (2009) Identification of cellular proteome modifications in response to West Nile virus infection. *Mol. Cell. Proteomics*, **8**, 1623–1637.
62. Geller,R., Taguwa,S. and Frydman,J. (2012) Broad action of Hsp90 as a host chaperone required for viral replication. *Biochim. Biophys. Acta*, **1823**, 698–706.
63. Kim,M.Y. and Oglesbee,M. (2012) Virus-heat shock protein interaction and a novel axis for innate antiviral immunity. *Cells*, **1**, 646–666.
64. Manzoor,R., Kuroda,K., Yoshida,R., Tsuda,Y., Fujikura,D., Miyamoto,H., Kajihara,M., Kida,H. and Takada,A. (2014) Heat shock protein 70 modulates influenza A virus polymerase activity. *J. Biol. Chem.*, **289**, 7599–7614.
65. Phillips,S.L., Soderblom,E.J., Bradrick,S.S. and Garcia-Blanco,M.A. (2016) Identification of proteins bound to Dengue viral RNA in vivo reveals new host proteins important for virus replication. *Mbio*, **7**, e01865–01815.
66. Vidalain,P.O. and Tangy,F. (2010) Virus-host protein interactions in RNA viruses. *Microbes Infect.*, **12**, 1134–1143.
67. Ortin,J. and Parra,F. (2006) Structure and function of RNA replication. *Annu. Rev. Microbiol.*, **60**, 305–326.
68. Rios-Marco,P., Romero-Lopez,C. and Berzal-Herranz,A. (2016) The cis-acting replication element of the Hepatitis C virus genome recruits host factors that influence viral replication and translation. *Sci. Rep.*, **6**, 25729.
69. Tao,Y.J. and Ye,Q. (2010) RNA virus replication complexes. *PLoS Pathog.*, **6**, e1000943.